# Cyanobacterial crowding-out effects on metabolite partitioning: modeling 2-methylisoborneol (MIB) release dynamics and implications

Yufan Ai<sup>a,d,#</sup> Yongnian Wu<sup>b,#</sup> Ming Su<sup>@,a,d,\*</sup> Yuying Gui<sup>a,c</sup> Yifan Du<sup>a</sup> Jiao Fang<sup>a</sup>

Tengxin Cao<sup>a,d</sup> Min Yang<sup>®,a,d</sup>

<sup>&</sup>lt;sup>#</sup> These authors contributed equally to this work.

<sup>&</sup>lt;sup>a</sup> Key Laboratory of Environmental Aquatic Chemistry, State Key Laboratory of Regional Environment and Sustainability, Research Center for Eco-Environmental Sciences, Chinese Academy of Sciences., Beijing 100085, China.

<sup>&</sup>lt;sup>b</sup> Bureau of Hydrology Information Center of Taihu Basin Authority, Shanghai 200434, China.

<sup>&</sup>lt;sup>c</sup> College of Environmental Science and Engineering, Ocean University of China, Qingdao 266100, China.

<sup>&</sup>lt;sup>d</sup> University of Chinese Academy of Sciences., Beijing 100049, China.

<sup>\*</sup> Corresponding to: Ming Su (mingsu@rcees.ac.cn)

#### **Abstract**

2-Methylisoborneol (MIB), a potent cyanobacterial metabolite, impairs drinking water quality through taste-and-odor issues at trace concentrations. Despite its significant impact, the intracellular dynamics and environmental release mechanisms of MIB remain poorly characterized. We developed a mechanistic model of growth-phase dependent MIB release through controlled experiments with two producer strains. The model reveals that the extracellular MIB proportion  $(f = e_{MIR}/t_{MIR})$  follows a consistent pattern: decreasing to a minimum at mid-log phase before rising and stabilizing (f: 0.4 to 0.6) during stationary phase, suggesting crowding-induced cell lysis drives release dynamics. Application of the model to Lake Taihu successfully reconstructed two odor events during 2022-2023, elucidating both the spatiotemporal development of MIB producers and identifying critical risk thresholds at ~15°C and >30°C under moderate light (0.1-0.4 mol m<sup>-2</sup> d<sup>-1</sup>) - patterns undetectable by conventional monitoring. Our findings demonstrate that physiological transitions, rather than just biomass accumulation, control odorant release. This framework may extend to other algal metabolites (e.g., geosmin, cyanotoxins), offering broader predictive capability. By linking cellular processes to water quality risks, our approach enables proactive management of cyanobacterial contaminants, informing both early warning systems and operational guidance for oxidant-type optimization to prevent large-scale release of hazardous compounds from algal cells.

## **Keywords**

2-methylisoborneol (MIB); Cell lysis-mediated release; Drinking water early warning; Growth-phase dependent release; Taste and odor.

### **I** Introduction

The issue of taste and odor (T&O) in drinking water sources is a major water quality concern, with earthy-musty odors caused by 2-methylisoborneol (MIB) being one of the most problematic problems [1–3]. MIB, an odorous terpenoid derivative, poses a persistent challenge in drinking water due to its extremely low odor threshold concentration (OTC) of 4 - 16 ng L<sup>-1</sup> and its resistance to conventional water treatment processes [4–12]. This compound is produced by various microorganisms, including actinomycetes [13, 14], cyanobacteria [15], fungi [16], and myxobacteria [17]. However, in drinking water sources, filamentous cyanobacteria—such as *Pseudanabaena*, *Planktothrix*, *Phormidium*, *Oscillatoria*, *Lyngbya*, and *Planktothricoides*—are the primary producers [18–23]. Unlike typical bloom-forming algae, MIB-producing cyanobacteria can thrive under moderate nutrient levels, intermediate light intensity, and temperatures of 20–30 °C, allowing them to grow even when conventional bloom species remain limited [24–28].

Following biosynthesis, MIB is primarily distributed inside the cells as intracellular MIB ( $i_{\rm MIB}$ ) or cell-bound MIB [29, 30]. It is then transported to the extracellular environment via cell membrane transporters, forming extracellular MIB ( $e_{\rm MIB}$ ). Additionally, MIB release can occur during cell wall rupture or lysis upon cell death [31, 32].

The distribution of MIB between intracellular and extracellular compartments has significant implications for drinking water treatment. If most MIB is already released into the water, advanced treatment processes such as ozone-activated carbon adsorption are required for its removal. Conversely, if MIB remains predominantly intracellular, conventional coagulation and sedimentation processes can effectively remove algal cells, or oxidants that minimize cell damage can be employed to prevent MIB release. Current monitoring practices in water treatment plants typically measure total MIB ( $t_{\rm MIB}$ ) without distinguishing between intracellular and extracellular fractions, limiting their utility in guiding treatment process selection. Previous studies have largely overlooked the intracellular and extracellular distribution of MIB, with most models focusing on its degradation kinetics and removal processes [33–36]. While some research has highlighted the surge in extracellular MIB during the senescent phase, attributing it to the rupture of algal filaments, the detailed relationship between extracellular MIB fluctuations and the growth cycle remains inadequately explored [37]. To date, no study has comprehensively described the trends in intracellular and extracellular MIB distribution or provided a thorough explanation for these changes.

Our observations from culture experiments suggest that the intracellular and extracellular distribution of MIB is not constant and may be influenced by its biosynthesis and release mechanisms [32, 37–39]. The biosynthetic pathway of MIB in cyanobacteria involves the methylation of geranyl diphosphate (GPP), followed by cyclization of methyl-GPP, catalyzed by 2-methylisoborneol synthase (2-MIBS) within the Sg Enc protein shell. Recent structural studies have revealed that the Sg Enc protein is a Family 2B encapsulin shell that self-assembles into an icosahedral nanocompartment, encapsulating 2-MIBS. [40–43]. However, due to the lack of observable pores in the Sg Enc shell and the challenges in directly tracking MIB migration, the mechanisms governing its release and distribution remain poorly understood.

MIB production in cyanobacteria is highly variable and influenced by environmental stressors

[25, 37]. While total MIB concentrations typically peak during the log growth phase and decline during the stationary phase, some studies report a negative correlation between MIB production and cell growth rates. For instance, *Pseudanabaena* sp. accumulates higher intracellular MIB and releases more extracellular MIB under suboptimal temperature and light conditions [32, 44, 45]. One hypothesis suggests that cyanobacteria may increase extracellular MIB release under stress to inhibit competing algal species, thereby maintaining ecological dominance [45]. Alternatively, extracellular MIB may simply result from cell damage or death under adverse conditions [32, 46].

In high-cell-density environments, crowding effects can restrict cell proliferation, migration, and metabolism, impacting growth and death dynamics [47–50]. Crowding-induced growth limitation arises from resource competition, spatial constraints, and cell cycle arrest [51, 52], while cell death may result from programmed cell death, metabolic stress, mechanical damage, or cell-to-cell interactions [53–55]. These effects indirectly influence the release of intracellular metabolites such as MIB.

The Logistic growth model effectively describes cyanobacterial population dynamics under crowding effects, incorporating intrinsic growth rate (r) and carrying capacity (K) to capture growth deceleration and inflection points [56–58]. This model is particularly useful for analyzing shifts in metabolic activity and the timing of metabolite release, making it well-suited for studying MIB dynamics [59, 60].

Based on these observations, we hypothesize that the ratio of  $e_{\rm MIB}$  to  $t_{\rm MIB}$  (f) is not constant but varies predictably over time in response to cell crowding. To test this, we developed a mechanistic model describing the temporal variation of f using culture experiments with typical MIB-producing strains. The goals of this work are (i) to explain MIB release patterns during cell growth, (ii) to assess growth-stage distributions of odor-producing cyanobacteria in Taihu Lake and predict odor risk during MIB outbreaks, and (iii) to provide new insights into MIB release dynamics, enhance understanding of cyanobacterial odor production, and offer practical guidance for water treatment process selection and bloom management.

### 2 Materials and Methods

## 2.1 Study Area and Sampling

Lake Taihu (30°55'40"–31°32'58" N, 119°52'32"–120°36'10" E), located in the southeastern Yangtze River Delta, is China's third-largest shallow freshwater lake, with a surface area of 2,578 km². The Taihu Lake watershed sustains a densely populated region of over 68 million people (2023 Bulletin on Water Resources in the Taihu Basin and Southeastern Rivers). The lake serves as a critical drinking water source for approximately 17 million residents, including about 20% of Shanghai's population. Since 2016, the newly constructed Jinze Reservoir has been supplying drinking water sourced from eastern Lake Taihu via the Taipu River. It is also extensively used for irrigation and aquaculture, making water quality a vital concern for local ecosystems and livelihoods. Considering the more widespread occurrence of MIB-related odor issues, and the fact that Lake Taihu serves as a major drinking water source, both MIB and GSM

have been routinely monitored. However, as GSM concentrations have consistently remained low while MIB has shown an increasing trend, MIB was selected as the primary focus of this study.

From March 2022 to February 2023, monthly water samples were collected from 31 sampling sites distributed across the lake (Fig. S1). Given the lake's average depth of ~2 m and well-mixed conditions, surface water samples (2 L) were collected from 0.5 m below the water surface using a Kemmerer water sampler. The water samples were sealed in brown narrow-mouth sampling bottles and taken to the laboratory for pretreatment within four hours.

### 2.2 Physicochemical Analysis and Phytoplankton Enumeration

In situ measurements of physicochemical parameters—including water temperature, pH, dissolved oxygen (DO), turbidity, and conductivity—were conducted using a multiparameter probe (EXO2, USA). Water transparency was quantified via Secchi depth (SD) measurements using a 20 cm diameter Secchi disk. Nutrient concentrations (nitrate, nitrite, ammonia, total nitrogen [TN], and total phosphorus [TP]) were analyzed following Chinese national standard methods (Ministry of Environmental Protection of PRC 2007, 2009, 2012, 2013).

For odorant analysis, subsamples (100 mL) were collected in amber glass bottles with airtight seals and preserved with 10 mg L<sup>-1</sup> HgCl<sub>2</sub> to inhibit biodegradation [61]. Total MIB production potential was determined by measuring its concentration within 72 hours using solid-phase microextraction (SPME) coupled with gas chromatography-mass spectrometry (GC-MS; Agilent 7890, USA) equipped with an Agilent VF-624ms column (USA), following established protocols [19, 35, 62].

For phytoplankton enumeration, subsamples (1000 mL) were fixed with 5% Lugol's iodine solution [63], settled for 48 hours, and pre-concentrated 20-fold before analysis. Cyanobacterial species were identified based on morphological criteria [64], with taxonomic revisions following ref [65]. Cell counts were performed using an upright microscope (Olympus BX53, Japan) following the Utermöhl method [66].

## 2.3 Model Development

The model was constructed on a Lenovo ThinkStation workstation (P350) running a Linux-based RStudio Server environment. The logistic growth model was applied to describe changes in cell density of cultured strains (Eq. 1):

$$N(t) = \frac{K}{1 + \frac{K - N_0}{N_0} e^{-rt}} \tag{1}$$

$$\theta = \frac{K - N_0}{N_0} \tag{2}$$

Here, K represents the environmental carrying capacity (maximum achievable cell density),  $N_0$  is the initial cell density (t = 0), r is the intrinsic growth rate (maximum growth rate under ideal conditions) [58, 60], and  $\theta$  denotes the initial growth potential. The Logistic model is based on the following key assumptions: (1) the algal population is considered a closed system, with no significant immigration or emigration; (2) external environmental conditions, such as nutrients, light, and temperature, remain relatively stable over the modeling period, or their effects are incorporated into the parameters; (3) biological processes, including predation, viral lysis, or other factors causing abrupt population declines, are assumed negligible; (4) the population is treated as homogeneous, with interspecies competition and internal physiological differences excluded.

In aquatic systems, MIB exists in two forms: intracellular ( $i_{\rm MIB}$ ) and extracellular ( $e_{\rm MIB}$ ), with their sum constituting total MIB ( $t_{\rm MIB}$ ). The ratio f ( $e_{\rm MIB}/t_{\rm MIB}$ ) serves as an odor index, reflecting the proportion of dissolved MIB over total MIB.

The odor-producing cyanobacterial strains Pseudanabaena cinerea FACHB 1277 (obtained from the Freshwater Algae Culture Collection at the Institute of Hydrobiology) and Planktothricoides raciborskii (isolated from the FH Reservoir in Zhuhai, China [25]) and maintained in BG-11 medium. Cultures were grown under controlled laboratory conditions (25 ± 1 °C, light intensity of 40  $\mu$ mol photons m<sup>-2</sup> s<sup>-1</sup>, 12:12 h light/dark cycle) and gently shaken daily to avoid cell sedimentation. The purity and identity of the strains were confirmed by routine microscopic examination, and no heterotrophic bacterial contamination was detected. Cell density was performed under a microscope (Olympus BX51, Japan) using a Sedgewick-Rafter counting chamber, and a cell counting tool (CCT v1.4, China, https://drwater.net) was used for recording and preliminary statistical analysis to determine growth phases (lag, exponential, stationary, and decline). These microbial tests ensured that the observed MIB release dynamics could be attributed specifically to cyanobacterial physiology rather than contamination from other microorganisms. To model temporal variations in  $e_{MIB}$  and  $t_{MIB}$  produced by Pseudanabaena cinerea FACHB 1277 and Planktothricoides raciborskii, we developed stage-specific equations for f. For cell densities below 80% of K (Phase I), f was derived from the logistic growth equation to capture early- to mid-growth dynamics (Eq. 3). For densities approaching K (>80%, Phase II), f was modeled using residual growth capacity to describe the stationary phase (Eq. 4):

$$f = 1 - \alpha_1 T \left( \frac{N(t)}{K} \right)' = 1 - \alpha_1 T \frac{\theta r e^{rt}}{e^{2rt} + 2\theta e^{rt} + \theta^2}$$
 (3)

$$f = \frac{1}{2} + \frac{K - N(t)}{K} \alpha_2 + \beta \tag{4}$$

Here,  $\alpha_1$  and  $\alpha_2$  are variation coefficients, T is the cell doubling time, and  $\beta$  serves as a correction factor representing the influence of physical and biological processes in the environment on MIB concentrations, such as degradation, volatilization, adsorption, and accumulation effects. Model parameters  $(N_0, K, r)$  were estimated via logistic curve fitting, while  $\alpha_1, \alpha_2$ , and  $\beta$  were

determined via linear regression. Adjusting r allowed simulation of growth and MIB production under varying environmental conditions.

#### 2.4 MIB Risk Assessment

For a given f, the cyanobacterial growth time (t) was derived from Eq. 3 and Eq. 4, and the growth stage indicator (St) was calculated as:

$$St = \frac{t}{2T_{IP}} \tag{5}$$

where  $T_{IP}$  (time at which N(t) = K/2) marks the logistic curve's inflection point. A smaller  $T_{IP}$  value indicates faster cyanobacterial growth and stronger crowding effects, thereby increasing the likelihood of cell rupture and MIB release. By combining St with field-measured  $t_{\rm MIB}$  concentrations, We performed a probabilistic analysis of St and  $t_{\rm MIB}$ , calculated the probability distribution of  $t_{\rm MIB}$  within each St interval, and used the expected value as the representative concentration for that interval. We generated a frequency distribution figure (Fig. S2) to quantify the probability of  $t_{\rm MIB}$  occurrence at different growth stages, enabling MIB risk evaluation.

### 2.5 Statistical Analysis and Visualization

All analyses were conducted in R 4.4.2 [67]. Data preprocessing and summarization used dplyr [68], while regression analyses (linear/generalized linear models) employed the stats package. Generalized additive modeling (mgcv [69]) and quantile regression (quantreg [70]) were applied where appropriate. Figures were generated using ggplot2 [71], with contour plots produced via the graphics package.

### 3 Results

# 3.1 Spatiotemporal Distribution Characteristics of MIB in Lake Taihu

Between March 2022 and February 2023, two severe MIB outbreaks were observed in Lake Taihu (Fig. 1A). The outbreaks exhibited distinct seasonal patterns, with elevated MIB concentrations occurring primarily in spring  $(40.0 \pm 77.5 \, \text{ng L}^{-1})$  and summer  $(107 \pm 230 \, \text{ng L}^{-1})$ . The highest peaks were recorded in April  $(66.5 \pm 101 \, \text{ng L}^{-1})$  and July  $(232 \pm 361 \, \text{ng L}^{-1})$ , demonstrating statistically significant seasonality (Fig. S3, p < 0.001).

Spatially, MIB distribution showed clear heterogeneity across the lake (Fig. 1B). The northern and southeastern regions consistently showed the highest concentrations, with the April peak centered in the northern area and the July peak affecting both northern and southeastern areas. Euclidean distance was used as the distance metric, and complete linkage was applied as the agglomeration method in the cluster analysis of MIB concentrations from all 31 sampling sites.

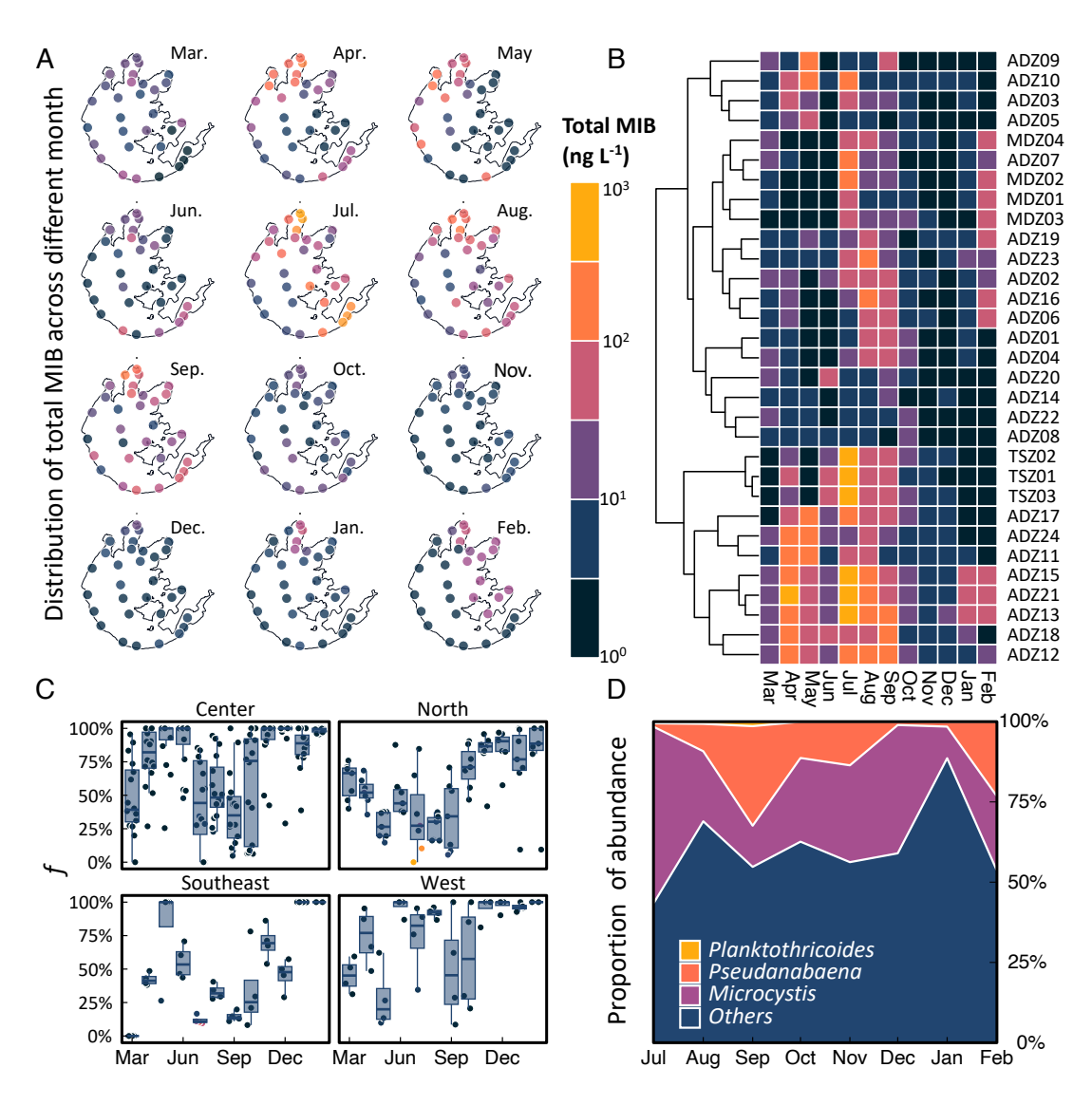


**Fig. 1:** Annual patterns of MIB and odor-producing cyanobacteria in Lake Taihu: (A) Spatiotemporal distribution of total MIB ( $t_{\text{MIB}}$ ) concentrations; (B) Spatial clustering of  $t_{\text{MIB}}$  concentrations across the lake; (C) Temporal variation in extracellular MIB proportion ( $e_{\text{MIB}}/t_{\text{MIB}}$ ) by lake region; (D) Seasonal shifts in dominant cyanobacterial genera composition.

This analysis revealed four distinct spatial clusters corresponding to different lake regions (West, Center, Southeast, and North) (Fig. S1).

Analysis of the f value variation across clusters revealed an important pattern: the lowest values during the log growth phase of f were typically followed by MIB outbreaks (Fig. 1C). Concurrent 16S RNA gene sequencing identified *Pseudanabaena* and *Planktothricoides* as the dominant MIB-producing genera, though their abundances varied significantly (Fig. S4). While *Microcystis* dominated the cyanobacterial community for most of the study period (Fig. 1D), *Pseudanabaena* reached its peak relative abundance (31.0%) in September. In contrast, *Planktothricoides* remained at much lower levels (1.4%).

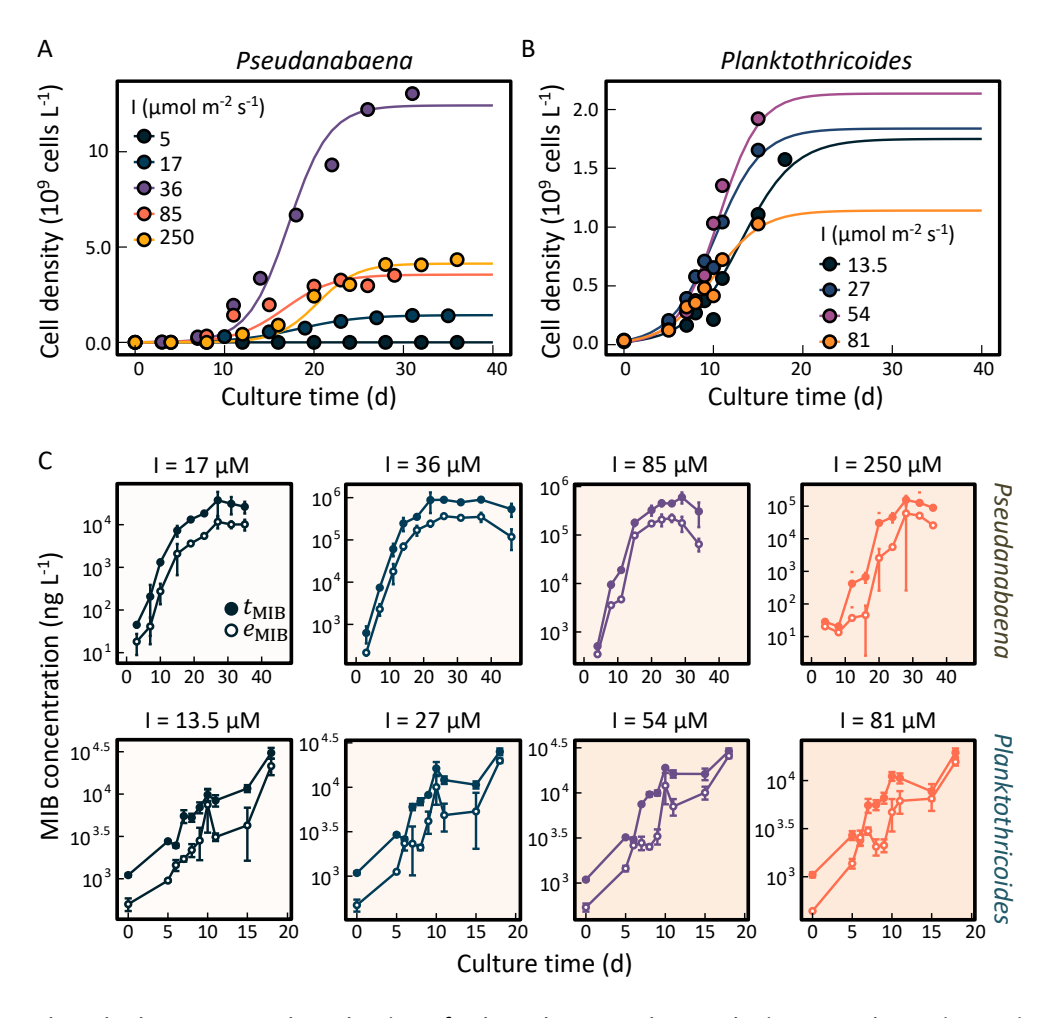


**Fig. 2:** Growth and odor compound production of cultured target odor-producing cyanobacteria: Logistic growth fitting for *Pseudanabaena* (A) and *Planktothricoides* (B), and corresponding MIB production patterns (C), with raw data from refs [27] and [25] respectively.

# 3.2 Modeling the Relationship Between Cultured Cyanobacteria Growth and Extracellular MIB Ratio (f)

The observed f ratio in Lake Taihu water samples exhibited a characteristic temporal pattern (Fig. 1C). To further elucidate this pattern, we analyzed the growth and odor production dynamics of two laboratory-cultured odor-producing cyanobacteria species (Pseudanabaena and Planktothricoides) under varying light conditions. A logistic growth-based model was developed to characterize the dynamics of the extracellular-to-total MIB ratio (f) (Eq. 3, Eq. 4). The model effectively captured the growth trajectories of both Pseudanabaena and Planktothricoides (Fig. 2A, 2B, Fig. S5, Fig. S6). Under different light regimes, both extracellular MIB ( $e_{\rm MIB}$ ) and total MIB ( $t_{\rm MIB}$ ) concentrations increased during the early growth phase (Fig. 2C), in parallel with rising cell densities. MIB production peaked when cell densities approached approximately half of the environmental carrying capacity (K), and remained relatively stable thereafter.

During growth and odor production, both species showed a consistent f ratio pattern: an initial

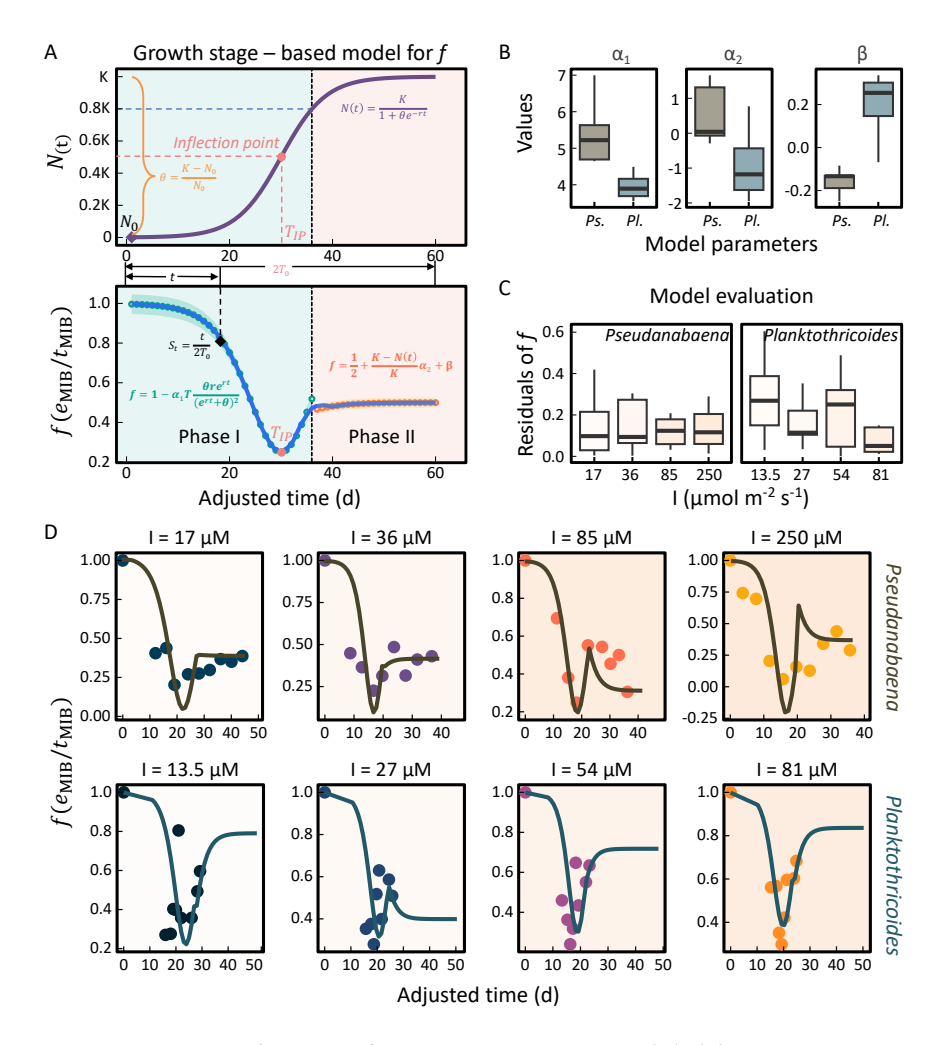


**Fig. 3:** Model development and performance for extracellular MIB ratio (f): (A) Logistic growth curve illustrating key growth phases and conceptual framework of the f ratio model; (B) Inter-species comparison of model parameters  $(\alpha_1, \alpha_1, \beta)$ ; (C) Model residual analysis for both species; (D) Modelled ratio (line) and observed ratio (circle) of extracellular MIB to total MIB (f) for cultured *Pseudanabaena* and *Planktothricoides*.

decrease reaching its minimum at approximately half of the maximum cell density, followed by a gradual increase that stabilized near 0.5. Notably, while  $e_{\text{MIB}}$  and  $t_{\text{MIB}}$  concentrations increased slowly during the initial phase, they rose rapidly during the subsequent phase of f ratio increase (Fig. 3A).

Parameter estimation revealed significant interspecies differences:  $\alpha_1$  was substantially higher for *Pseudanabaena* than for *Planktothricoides* (p < 0.01), while  $\beta$  showed the opposite trend (p < 0.01) (Fig. 3B). The model demonstrated good overall performance, with relatively small residuals across most growth conditions (Fig. 3C). Under varying light conditions, the observed changes in the f values of the two cultured odor-producing cyanobacteria were well captured by the model-derived f value curves (Fig. 3D). Moreover, despite differences in species and experimental conditions, the f value trajectories exhibited similar patterns across treatments. Specifically, in the first phase, the f value declined and then increased, while in the second phase, it fluctuated before stabilizing at a relatively constant level (Fig. 3A, Fig. S7).

# 3.3 Spatiotemporal Variation of Odor-Producing Cyanobacteria Growth Stages in Lake Taihu

The dominant odor-producing cyanobacterium *Pseudanabaena* in Lake Taihu exhibited high cell densities from July to October, followed by a significant decline starting in November (Fig. S8). Among all regions, the northern and southeastern parts of the lake consistently showed higher *Pseudanabaena* cell densities. Notably, some sites in the northern region still recorded cell densities exceeding 10<sup>5</sup> cells L<sup>-1</sup> as late as December and the following January.

Field monitoring of algae has shown that Pseudanabaena is the main odor-producing cyanobacterium. Therefore, when applying the model to Lake Taihu, MIB is assumed to be solely produced by Pseudoanabaena. The cultivation-based model was successfully applied to field data from sampling locations throughout Lake Taihu to characterize growth parameters and determine St values for odor-producing cyanobacteria. Analysis revealed two distinct seasonal growth patterns across the lake. A primary growth phase developed from May through November as water temperatures increased, followed by a secondary, smaller-scale growth phase (St) occurring between December and April after winter production (Fig. 4A). Examination of algal growth stages across different cluster regions demonstrated strong synchronization between cyanobacterial growth dynamics and MIB outbreak events (Fig. 4B).

To enable broader application of the model across Lake Taihu, we compiled data on water temperature, solar radiation, and odor-producing cyanobacteria growth patterns under various conditions from multiple sources (Table S1, Fig. S9, Fig. S10). By analyzing these monthly variations, we established relationships between environmental factors (temperature and light intensity) and the intrinsic growth rate (r) of cyanobacteria. Our analysis revealed clear seasonal differences in the distribution of cyanobacterial growth stages (Fig. 5A). From spring (March 2022) through winter (February 2023), the growth stages followed a consistent pattern of initial increase followed by gradual decline across the entire lake. Spatially, the northern and southeastern regions consistently showed more advanced growth stages compared to other areas throughout all seasons.

The seasonal progression of growth stages exhibited distinct spatial patterns. In early spring, odor-producing cyanobacteria first began growing in the northwest and southeast regions. By summer, active growth had spread to most areas of the lake. During autumn, the northern, southern and southeastern regions reached later growth stages, while in winter, cyanobacterial growth became minimal across nearly the entire lake, with only a small portion of the northern region showing any activity.

The relationship between odor-producing cyanobacteria growth stage (St) and total MIB concentration  $(t_{\text{MIB}})$  was further analyzed to assess annual odor risk distribution in Lake Taihu (Fig. 5B, Fig. S11). The analysis revealed similar spatial patterns for the probability of MIB exceeding both 10 ng L<sup>-1</sup> and 50 ng L<sup>-1</sup> thresholds, with the higher threshold's probability typically being half that of the lower threshold.

Seasonal risk patterns showed elevated MIB concentrations occurring during two main periods: spring (March-May) and late summer through autumn (July-October). June represented a transitional period between these two risk episodes, while from November to February, most of the

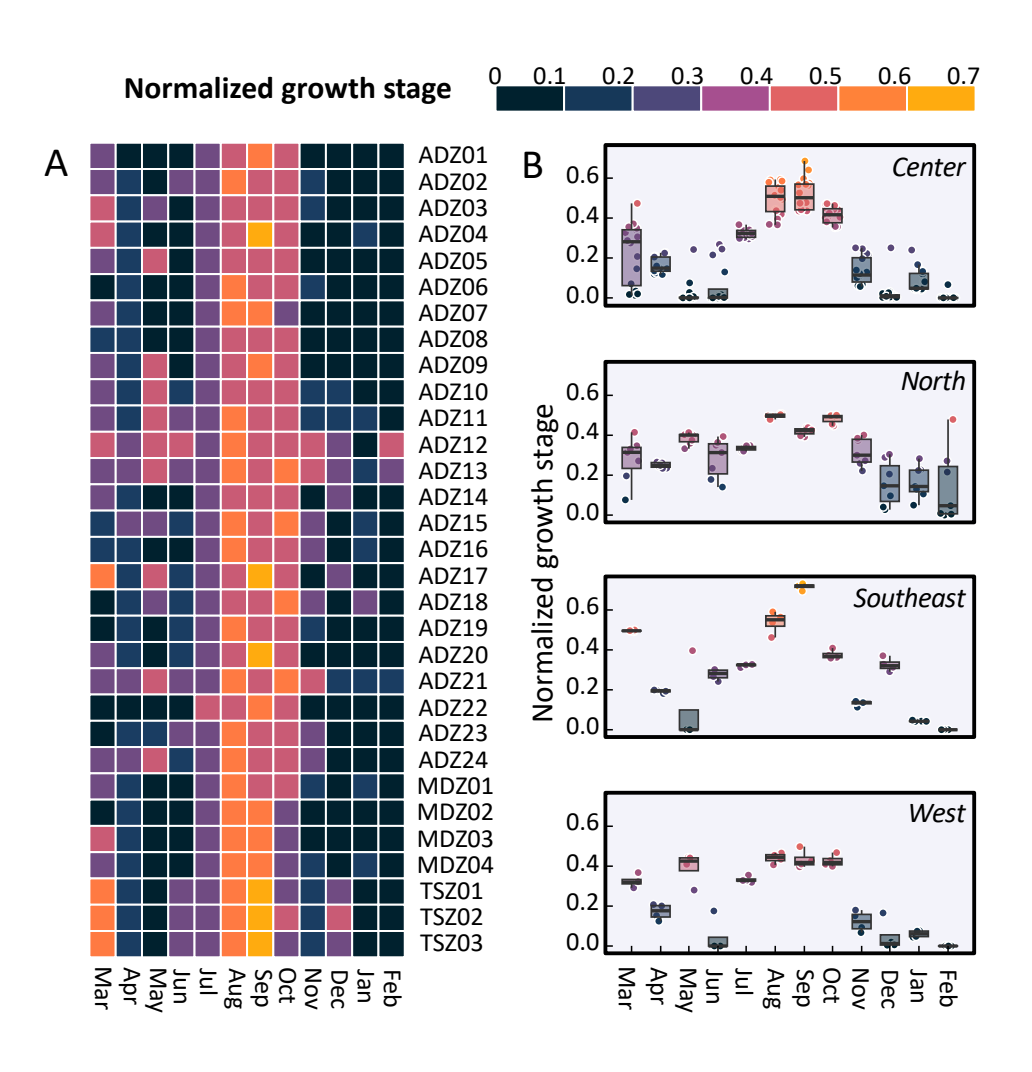


**Fig. 4:** Growth stage of odor-producing cyanobacteria determined by the f model in the Lake Taihu (A) and different subregions (B).

lake showed minimal risk except for localized areas in the northern and southeastern regions.

Spatially, spring risks were primarily concentrated in the northern lake region. During late summer and autumn, high-risk areas expanded to encompass nearly the entire lake. Throughout all seasons, the northern and southeastern regions consistently emerged as high-probability hotspots for elevated MIB concentrations.

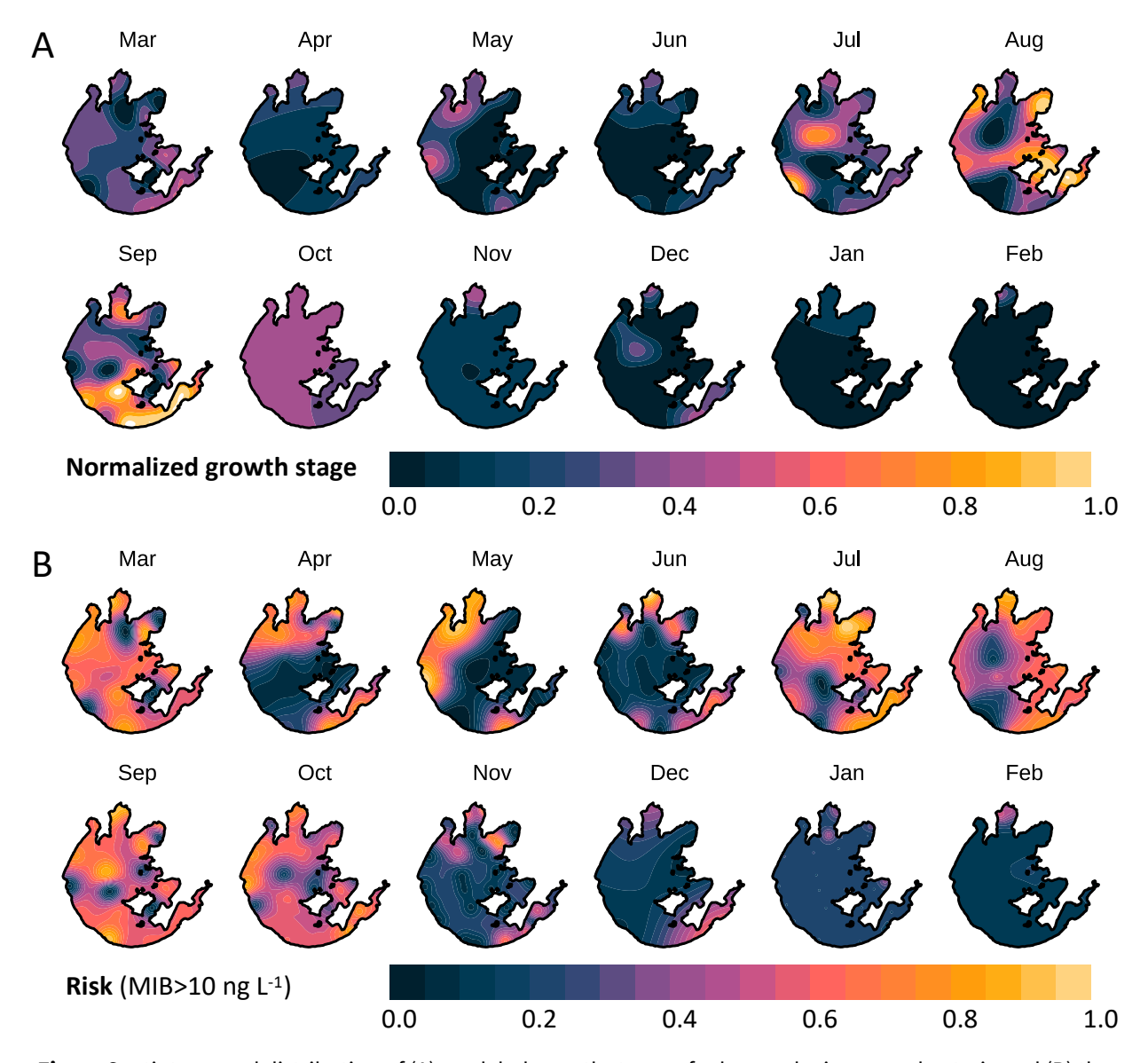


**Fig. 5:** Spatiotemporal distribution of (A) modeled growth stages of odor-producing cyanobacteria and (B) the risk of MIB occurrence (probability of  $t_extMIB > 10$  ng L<sup>-1</sup>) in Lake Taihu.

#### 4 Discussion

# 4.1 High-risk conditions for rapid MIB-producer growth and crowding-induced release

Understanding the environmental conditions that promote rapid growth and crowding of odor-producing cyanobacteria is essential for predicting MIB risk dynamics in source waters. Our analysis reveals that the inflection point time  $(T_{IP})$  from logistic growth modeling serves as a robust indicator of when cyanobacterial populations reach critical densities associated with elevated MIB release risk. Shorter  $T_{IP}$  values indicate faster growth rates and earlier onset of crowding effects, ultimately leading to MIB release and higher extracellular concentrations.

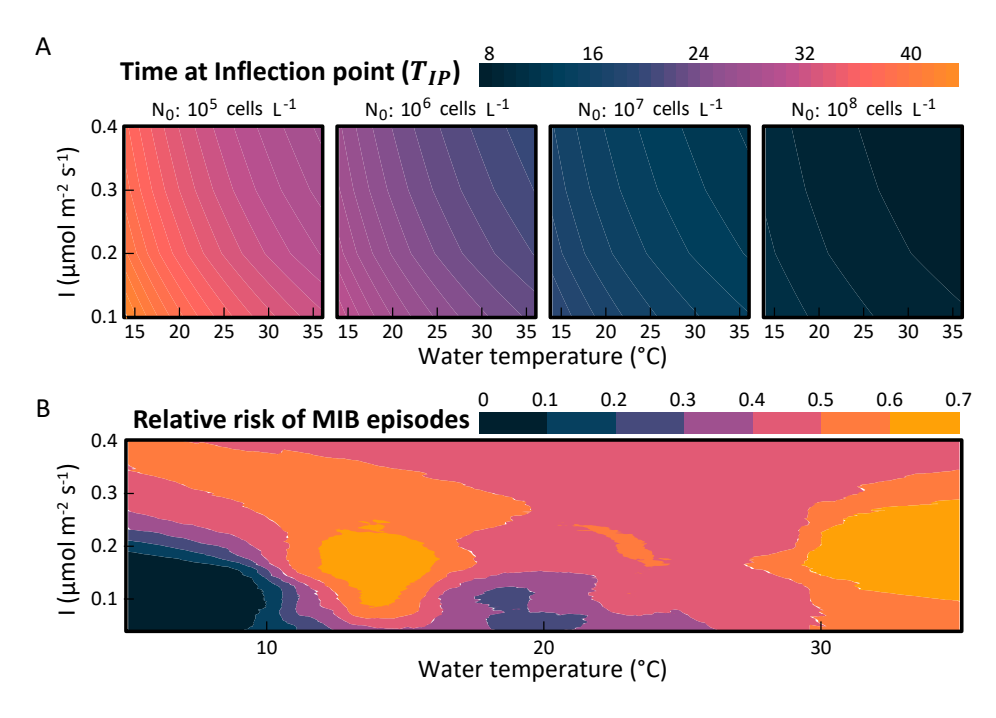


**Fig. 6:** Modeled relationships between inflection point time  $(T_{IP})$ , MIB risk, and environmental drivers in Lake Taihu: (A) Mechanistic model outputs showing  $T_{IP}$  as a function of water temperature, underwater light dose (I), and initial cell density  $(N_0)$ ; (B) Estimated probability of MIB concentrations exceeding the 10 ng  $L^{-1}$  threshold under identified high-risk conditions.

Field observations from Lake Taihu demonstrate that  $T_{IP}$  shows consistent negative correlations with three key environmental factors: initial cell density, light availability, and temperature within typical lake conditions (15-35°C; 0.1-0.4 mol m<sup>-2</sup> d<sup>-1</sup> underwater light, Fig. 6A). When carrying capacity remains stable, higher initial cell densities substantially shorten the growth stage duration, accelerating the progression to crowding conditions. Similar acceleration occurs under favorable light and temperature conditions, where increased light intensity and warmer temperatures enhance growth rates, reducing  $T_{IP}$  and promoting earlier cell lysis and odor compound release.

These relationships explain the characteristic bimodal pattern of MIB events in Lake Taihu, with risk peaks occurring at approximately 15°C and above 30°C under moderate light conditions (Fig. 6B). The model outputs confirm that temperature-mediated changes in cyanobacterial growth dynamics represent the primary driver of seasonal MIB risk variations, matching historical patterns of spring and summer odor outbreaks in the lake.

# 4.2 Modeling MIB Partitioning Dynamics in Relation to Cyanobacterial Growth Phases

The production and distribution of 2-methylisoborneol (MIB) by odor-producing cyanobacterial cells are influenced by both their growth stage and environmental stressors. Previous studies have rarely focused on the intracellular and extracellular distribution of MIB during the growth of cyanobacteria in both natural aquatic environments and laboratory cultures. Some even sug-

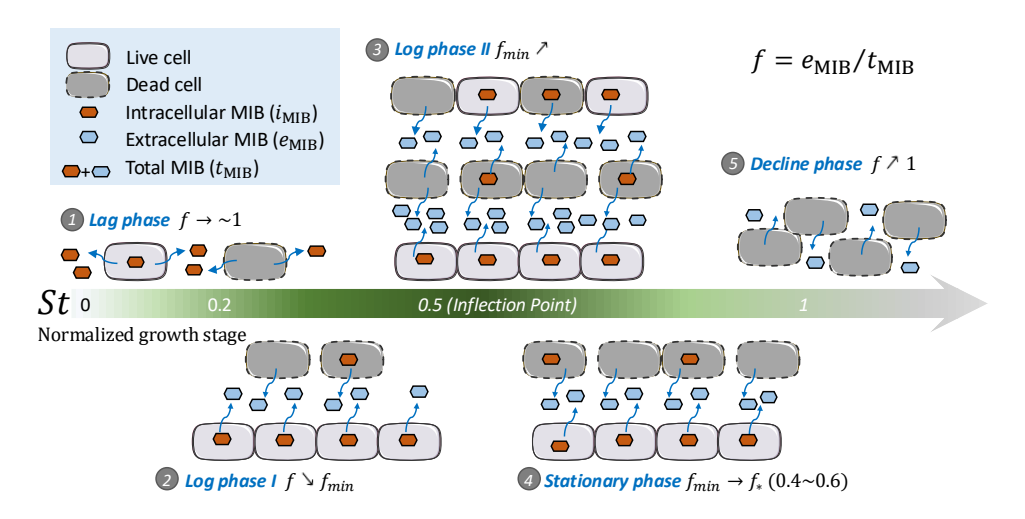


**Fig. 7:** Schematic representation of MIB allocation dynamics influenced by cell crowding, both intracellularly and extracellularly

gested that the variation in MIB partitioning lacks a discernible pattern [72, 73]. In this study, we introduce the ratio  $f\left(e_{MIR}/t_{MIR}\right)$  as a key indicator to represent the distribution pattern of MIB. Our findings show that f is not a constant, but follows a specific dynamic trend, which is mainly attributed to cell crowding effects (Fig. 7). After synthesis, MIB is primarily bound to cytoplasmic and soluble protein fractions within cyanobacterial cells [74]. The major mechanism of MIB release is cell lysis, occurring either through programmed cell death or mechanical rupture of the cell wall [32, 37, 39, 46]. In this study, we established a model describing the relationship between f and growth time t, and further proposed a metric—growth stage (St)—to evaluate the distribution of cyanobacterial growth stages across the lake (Fig. 7). The St index ranges from 0 to 1, representing the progression of cell growth from the lag phase to the stationary phase, with St = 0.5 corresponding to the inflection point of the logistic growth curve. A higher St indicates a larger proportion of cells in the later stages of growth, implying a greater potential for MIB release. The St values proved particularly informative, as values approaching 0.5 reliably indicated when populations reached the inflection point of logarithmic growth - a critical threshold associated with elevated risk of substantial MIB release. As cell growth progresses toward the stationary phase, environmental cell density increases, leading to intensified crowding effects. These conditions exacerbate cell damage and apoptosis, causing a larger proportion of MIB to be released into the surrounding water [75]. When applying the model to real aquatic systems, monocultures of odor-producing cyanobacteria are more suitable. In mixed cultures, it is difficult to determine the contribution of each species to the odor compounds, which limits the model's applicability. Additionally, compared to laboratory conditions, variations in meteorological factors and community interactions in natural environments may affect the model's performance, highlighting areas for future improvement.

Our model enables the estimation of the growth stage distribution of odor-producing cyanobacteria, offering insights into current odor issues and supporting prediction of future taste and odor (T&O) risks. From a management perspective, f serves dual functions: (1) as a T&O index reflecting the proportion of dissolved MIB ( $e_{\text{MIB}}$ ) to total MIB ( $t_{\text{MIB}}$ ) in the water, and (2) as an

ecological indicator of the relative proportions of cells at different growth stages. Model results (Fig. 2A, B) demonstrate that f follows a nonlinear pattern—initially decreasing, then increasing and eventually stabilizing—as the cell population transitions from the lag phase to the stationary phase. During the log phase, f reaches its minimum when cell growth rate peaks at the inflection point of the logistic growth curve. After this point, crowding-induced stress increases, leading to significant MIB release due to cell damage and apoptosis. Toward the end of the log phase and during the stationary phase, cell density approaches the environmental carrying capacity and enters a state of dynamic equilibrium. At this stage, f is primarily influenced by total cell density and the accumulation and degradation dynamics of  $e_{\rm MIB}$  in the environment. This trend is consistent with observations reported in previous studies [32, 37]. By applying the f-model, the growth stage distribution of odor-producing cyanobacteria can be inferred based on measured MIB partitioning. This framework enhances our understanding of T&O events in freshwater lakes and reservoirs and provides valuable guidance for implementing more targeted management strategies. However, in real aquatic environments, the ideal conditions assumed by the model are often not fully met. For example, water exchange may introduce new cells or dilution effects, and nutrient pulses or light fluctuations can lead to time-varying growth rates and environmental carrying capacities. In the future, to enhance the model's applicability, further adjustments and optimizations may be necessary, such as introducing time-varying carrying capacity K(t), adding migration terms, or considering predation loss functions.

# 4.3 Field-Based Analysis of MIB Dynamics in Relation to Cyanobacterial Growth in Lake Taihu

Analysis of intracellular and extracellular MIB distribution patterns, influenced by cell crowding effects, provides insights into the growth dynamics and odor production processes of MIB-producing cyanobacteria in Lake Taihu. Lake-wide distribution of St values revealed that cyanobacterial growth initiates during the winter-spring transition in specific areas, beginning with slow early-phase growth that continues until early summer, followed by accelerated growth through late autumn. This bimodal MIB pattern shows temporal variations across years. For example, monitoring data from 2019 and 2021 documented smaller May peaks (predominantly in the southeastern region) alongside major August peaks [76, 77]. Temperature and light availability emerge as the principal environmental regulators of this pattern. When surface water temperatures exceed 15°C in April-May, MIB-producing cyanobacteria achieve substantial growth rates [78-80], benefiting from minimal competition and resulting in spring MIB peaks. In the Shanghai QCS Reservoir, located at the same latitude, an MIB outbreak caused by Pseudoanabaena was observed at the end of April [27]. Subsequent Microcystis blooms (May-July) reduce light availability in subsurface layers where filamentous MIB producers reside, temporarily suppressing their growth [81, 82]. Summer conditions typically optimize growth for Pseudanabaena, when the temperature rises to 30°C, odor-producing cyanobacteria gain a competitive advantage over traditional bloom-forming algae, resulting in an increased odor risk [77, 81, 83, 84]. This ecological succession aligns with observed microcystin concentration trends [76] and documented phytoplankton community shifts [85].

High-risk zone analysis reveals distinct spatiotemporal patterns between northern and southeastern regions. The southeastern zone showed modest April increases followed by July peaks persisting through September, while the northern region exhibited stronger spring peaks with sustained MIB levels (>10 ng L<sup>-1</sup>) between major outbreaks. These differences reflect contrasting cyanobacterial growth dynamics: southeastern populations transitioned from late-growth phase in March to early growth by April, suggesting significant cell mortality and limited MIB production potential, whereas northern populations maintained log-phase growth through spring with correspondingly higher production potential. The observed north-to-south progression of odor risk zones represents a previously unreported spatial-temporal pattern in Lake Taihu's MIB dynamics.

Species-specific analyses demonstrate considerable variation in growth and MIB production characteristics. Model parameterization revealed significant interspecies differences (Fig. 2E), attributable to variations in intrinsic growth rates and MIB production efficiencies. Where  $\alpha_1$  represents the coefficient between the rate of change in f with respect to cell density, indicating the magnitude of the crowding effect on the intracellular-extracellular distribution of MIB as the cell growth stage progresses, and is influenced by the cell growth rate.  $\beta$  represents the correction factor for MIB degradation or accumulation effects, and is related to the odor production efficiency of individual cells. Comparative studies show *Pseudanabaena* achieves maximum cellular MIB yields of 0.15 ± 0.04 pg cell<sup>-1</sup> under 85  $\mu$  mol photons m<sup>-2</sup> s<sup>-1</sup> [27], while *Planktothricoides* reaches 0.22 ± 0.02 pg cell<sup>-1</sup> under similar conditions [25]. These physiological differences, combined with variations in population growth inflection points ( $T_{IP}$ ) across studies (Fig. S12), contribute to species-specific impacts on odor event dynamics.

### 5 Conclusion

The intracellular and extracellular distribution dynamics of 2-methylisoborneol (MIB), a mustysmelling secondary metabolite produced by cyanobacteria, remain poorly understood, limiting our ability to predict odor events in source waters. This study developed a growth-stagebased model to characterize MIB release patterns and applied it to Lake Taihu, where conventional approaches have struggled to explain complex odor phenomena. Results revealed that odor-producing cyanobacteria in the lake underwent two distinct growth cycles annually, corresponding to dual MIB concentration peaks—in spring and summer. The f model, derived from laboratory-cultured cyanobacteria data, accurately captured these growth trends and was successfully applied to field observations across the lake. By integrating environmental variables such as water temperature and light intensity, the model enabled lake-wide prediction of cyanobacterial growth stages and corresponding MIB risk. Spatially, the northern and southeastern regions of Lake Taihu consistently showed higher growth potential and odor risk. Temporally, high MIB risk was concentrated in early spring and mid-summer, aligning with inflection points in the cyanobacterial growth phase. Further analysis indicated that environmental factors—especially temperature and light dose—significantly influenced the timing of growth phase transitions, thereby affecting odor risk. Notably, the model identified two risk peaks under moderate light conditions, reflecting the dual seasonal odor patterns observed in the lake. These findings demonstrate the applicability of the f model as a predictive tool for early MIB warnings and provide valuable insights for water quality monitoring and lake management.

## **Environmental Implication**

This study presents a mechanistic model linking cyanobacterial growth stages with the release and partitioning of 2-methylisoborneol (MIB) into intracellular and extracellular fractions. Applied to Lake Taihu, the model enables spatial prediction of odor risk and informs targeted water treatment strategies. By distinguishing dominant MIB forms, it supports the selection of appropriate control measures—coagulation-based cell removal or advanced oxidation for dissolved MIB. This framework enhances early warning capability and provides actionable guidance for managing taste and odor issues in freshwater systems affected by cyanobacterial blooms.

## **CRediT** authorship contribution statement

**Yufan Ai:** Conceptualization, Methodology, Data curation, Formal analysis, Writing – original draft, Writing – review & editing. **Yongnian Wu:** Methodology, Data curation, Writing – original draft, Writing – review & editing. **Ming Su:** Conceptualization, Formal analysis, Project administration, Supervision, Visualization, Writing – original draft, Writing – review & editing. **Yuying Gui:** Methodology, Formal analysis. **Yifan Du:** Methodology, Formal analysis. **Jiao Fang:** Methodology, Formal analysis. **Tengxin Cao:** Methodology, Formal analysis. **Min Yang:** Conceptualization, Supervision, Validation, Project administration, Resources.

## **Declaration of competing interest**

The authors declare no competing financial interest.

## **Acknowledgments**

This work was financially supported by the National Natural Science Foundation of China (52030002, W2412156, 51878649) and the National Key R&D Program of China (2023YFC3207804, 2022YFC3203603), Shanghai Municipal Investment (Group) Corporation (CTKY-ZDZX-2023-004).

## **Supplementary materials**

Supplementary material associated with this article can be found, in the online version, at doi:XXX.

## **Data availability**

Data used for analysis will be made available on request. The R scripts for analyses of this study is available on https://git.drwater.net/codes/ai2025cyanobacterial.git

### References

- [1] WHO WHO, 2011. Guidelines for Drinking-Water Quality. World Health Organization, Geneva, Switzerland
- [2] Devi A, Chiu Y-T, Hsueh H-T, Lin T-F, 2021. Quantitative PCR based detection system for cyanobacterial geosmin/2-methylisoborneol (2-MIB) events in drinking water sources: Current status and challenges. Water Research 188, 116478. https://doi.org/10.1016/j. watres.2020.116478
- [3] Suurnäkki S, Gomez-saez GV, Rantala-ylinen A, Jokela J, Fewer DP, Sivonen K, 2015. Identification of geosmin and 2-methylisoborneol in cyanobacteria and molecular detection methods for the producers of these compounds. Water Research 68, 56–66. https://doi.org/10.1016/j.watres.2014.09.037
- [4] Izaguirre G, Taylor WD, 2004. A guide to geosmin- and MIB-producing cyanobacteria in the united states. Water Science and Technology 49, 19–24. https://doi.org/10.2166/wst. 2004.0524
- [5] Wang C, An W, Zhao Y, Dietrich AM, Gallagher DL, Zhang Y, Qian Y, Yu J, Yang M, 2023. Risk assessment for 2-MIB odor complaint in drinking water based on zero-inflated log-normal model. ACS ES&T Water 4, 146–154. https://doi.org/10.1021/acsestwater. 3c00477
- [6] Suffet Ih (mel), Khiari D, Bruchet A, 1999. The drinking water taste and odor wheel for the millennium: Beyond geosmin and 2-methylisoborneol. Water Science and Technology 40, 1–13. https://doi.org/10.1016/s0273-1223(99)00531-4
- [7] Gillogly TET, Snoeyink VL, Newcombe G, Elarde JR, 1999. A simplified method to determine the powdered activated carbon dose required to remove methylisoborneol. Water Science and Technology 40, 59–64. https://doi.org/10.1016/S0273-1223(99)00538-7
- [8] Dionigi CP, Millie DF, Johnsen PB, 1991. Effects of farnesol and the off-flavor derivative geosmin on *Streptomyces Tendae*. Applied and Environmental Microbiology 57, 3429–3432
- [9] Lin T-F, Wong J-Y, Kao H-P, 2002. Correlation of musty odor and 2-MIB in two drinking water treatment plants in south taiwan. Science of the Total Environment 289, 225–235. https://doi.org/10.1016/S0048-9697(01)01049-X
- [10] Li L, Yang S, Yu S, Zhang Y, 2019. Variation and removal of 2-MIB in full-scale treatment plants with source water from Lake Tai, China. Water Research 162, 180–189. https://doi.org/10.1016/j.watres.2019.06.066

- [11] AWWA AWWA, 2010. Algae: Source to treatment. American Water Works Association
- [12] Cerón-Vivas A, Villamizar León MP, Cajigas ÁA, 2022. Geosmin and 2-methylisoborneol removal in drinking water treatment. Water Practice and Technology 18, 159–167. https://doi.org/10.2166/wpt.2022.167
- [13] Gerber NN, 1969. A volatile metabolite of actinomycetes, 2-methylisoborneol. Antibiotics 22, 508–509
- [14] Franklin HM, Podduturi R, Jørgensen NOG, Roberts DT, Schlüter L, Burford MA, 2023. Potential sources and producers of 2-methylisoborneol and geosmin in a river supplying a drinking water treatment plant. Chemical Engineering Journal Advances 14, 100455. https://doi.org/10.1016/j.ceja.2023.100455
- [15] Tabachek JL, Yurkowski M, 1976. Isolation and identification of blue-green algae producing muddy odor metabolites, geosmin, and 2-methylisoborneol, in saline lakes in Manitoba. Journal of the Fisheries Research Board of Canada 33, 25–35. https://doi.org/10.1139/f76-004
- [16] Yamada Y, Kuzuyama T, Komatsu M, Shin-ya K, Omura S, Cane DE, Ikeda H, 2014. Terpene synthases are widely distributed in bacteria. Proceedings of the National Academy of Sciences 112, 857–862. https://doi.org/10.1073/pnas.1422108112
- [17] Dickschat Jeroen s, Nawrath T, Thiel V, Kunze B, Müller R, Schulz S, 2007. Biosynthesis of the off-flavor 2-methylisoborneol by the myxobacterium nannocystis exedens. Angewandte Chemie International Edition 46, 8287–8290. https://doi.org/10.1002/anie. 200702496
- [18] Su M, Suruzzaman MD, Zhu Y, Lu J, Yu J, Zhang Y, Yang M, 2021. Ecological niche and insitu control of MIB producers in source water. Journal of Environmental Sciences 110, 119–128. https://doi.org/10.1016/j.jes.2021.03.026
- [19] Su M, Yu J, Zhang J, Chen H, An W, Vogt RD, Andersen T, Jia D, Wang J, Yang M, 2015. MIB-producing cyanobacteria (*Planktothrix* sp.) in a drinking water reservoir: Distribution and odor producing potential. Water Research 68, 444–453. https://doi.org/10.1016/j. watres.2014.09.038
- [20] Lu J, Su M, Su Y, Fang J, Burch M, Cao T, Wu B, Yu J, Yang M, 2023. MIB-derived odor management based upon hydraulic regulation in small drinking water reservoirs: Principle and application. Water Research 244, 120485. https://doi.org/10.1016/j.watres.2023. 120485

- [21] Izaguirre G, Jungblut A, Neilan BA, 2007. Benthic cyanobacteria (oscillatoriaceae) that produce microcystin-LR, isolated from four reservoirs in Southern California. Water Research 41, 492–498. https://doi.org/10.1016/j.watres.2006.10.012
- [22] Van Der Ploeg M, Dennis M, De Regt M, 1995. Biology of *Oscillatoria chalybea*, a 2-methylisoborneol producing blue-green alga of Mississippi Catfish Ponds. Water Science and Technology 31, 173–180. https://doi.org/10.1016/0273-1223(95)00473-Z
- [23] Jüttner F, Watson SB, 2007. Biochemical and ecological control of geosmin and 2-methylisoborneol in source waters. Applied and Environmental Microbiology 73, 4395–4406. https://doi.org/10.1128/aem.02250-06
- [24] Su M, Yu J, Pan S, An W, Yang M, 2014. Spatial and temporal variations of two cyanobacteria in the mesotrophic Miyun Reservoir, China. Journal of Environmental Sciences 26, 289–298. https://doi.org/10.1016/s1001-0742(13)60433-7
- [25] Lu J, Su M, Su Y, Wu B, Cao T, Fang J, Yu J, Zhang H, Yang M, 2022. Driving forces for the growth of MIB-producing *Planktothricoides raciborskii* in a low-latitude reservoir. Water Research 118670. https://doi.org/10.1016/j.watres.2022.118670
- [26] Zhang T, Li L, Song L, Chen W, 2009. Effects of temperature and light on the growth and geosmin production of *Lyngbya kuetzingii* (cyanophyta). Journal of Applied Phycology 21, 279–285. https://doi.org/10.1007/s10811-008-9363-z
- [27] Cao T, Fang J, Jia Z, Zhu Y, Su M, Zhang Q, Song Y, Yu J, Yang M, 2023. Early warning of MIB episode based on gene abundance and expression in drinking water reservoirs. Water Research 231, 119667. https://doi.org/https://doi.org/10.1016/j.watres.2023.119667
- [28] Clercin NA, Druschel GK, 2019. Influence of environmental factors on the production of MIB and geosmin metabolites by bacteria in a eutrophic reservoir. Water Resources Research 55, 5413–5430. https://doi.org/10.1029/2018wr023651
- [29] Bentley R, Meganathan R, 1981. Geosmin and methylisoborneol biosynthesis in streptomycetes. Evidence for an isoprenoid pathway and its absence in non-differentiating isolates. FEBS Letters 125, 220
- [30] Wu J, Jüttner F, 1988. Differential partitioning of geosmin and 2-methylisoborneol between cellular constituents in *Oscillatoria tenuis*. Archives of Microbiology 150, 580–583. https://doi.org/10.1007/bf00408253
- [31] Rashash DmC, Dietrich Am, Hoehn Rc, Parker Bc, 1995. The influence of growth conditions on odor-compound production by two chrysophytes and two cyanobacteria. Water Science and Technology 31, 165–172. https://doi.org/10.1016/0273-1223(95)00472-y

- [32] Zhang T, Zheng L, Li L, Song L, 2016. 2-methylisoborneol production characteristics of *Pseudanabaena* sp. FACHB 1277 isolated from Xionghe Reservoir, China. Journal of Applied Phycology 1–10. https://doi.org/10.1007/s10811-016-0864-x
- [33] Cook D, Newcombe G, Sztajnbok P, 2001. The application of powdered activated carbon for MIB and geosmin removal: Predicting PAC doses in four raw waters. Water Research 35, 1325–1333. https://doi.org/10.1016/S0043-1354(00)00363-8
- [34] Li L, Zhu C, Xie C, Shao C, Yu S, Zhao L, Gao N, 2018. Kinetics and mechanism of *Pseudoanabaena* cell inactivation, 2-MIB release and degradation under exposure of ozone, chlorine and permanganate. Water Research 147, 422–428. https://doi.org/10.1016/j.watres. 2018.10.023
- [35] Pan L, Nakayama A, Matsui Y, Matsushita T, Shirasaki N, 2022. Desorption of micropollutant from superfine and normal powdered activated carbon in submerged-membrane system due to influent concentration change in the presence of natural organic matter: Experiments and two-component branched-pore kinetic model. Water Research 208, 117872. https://doi.org/10.1016/j.watres.2021.117872
- [36] Mustapha S, Tijani JO, Ndamitso M, Abdulkareem AS, Shuaib DT, Mohammed AK, 2021. A critical review on geosmin and 2-methylisoborneol in water: Sources, effects, detection, and removal techniques. Environmental Monitoring and Assessment 193. https://doi.org/10.1007/s10661-021-08980-9
- [37] Wang H, Li L, Cheng S, Chen L, Zhang H, Zhang X, 2024. Production and release of 2-MIB in *Pseudanabaena*: Effects of growth phases on cell characteristics and 2-MIB yield. Ecotoxicology and Environmental Safety 274, 116198. https://doi.org/10.1016/j.ecoenv. 2024.116198
- [38] Oh H-S, Lee CS, Srivastava A, Oh H-M, Ahn C-Y, 2017. Effects of environmental factors on cyanobacterial production of odorous compounds: Geosmin and 2-methylisoborneol. Journal of Microbiology and Biotechnology 27, 1316–1323. https://doi.org/10.4014/jmb. 1702.02069
- [39] Alghanmi HA, Alkam FM, AL-Taee MM, 2018. Effect of light and temperature on new cyanobacteria producers for geosmin and 2-methylisoborneol. Journal of Applied Phycology 30, 319–328. https://doi.org/10.1007/s10811-017-1233-0
- [40] Giglio S, Chou WKW, Ikeda H, Cane DE, Monis PT, 2011. Biosynthesis of 2-methylisoborneol in cyanobacteria. Environmental Science & Technology 45, 992–998. https://doi.org/10.1021/es102992p

- [41] Wang Z, Xu Y, Shao J, Wang J, Li R, 2011. Genes associated with 2-methylisoborneol biosynthesis in cyanobacteria: Isolation, characterization, and expression in response to light. Plos One 6, E18665. https://doi.org/10.1371/journal.pone.0018665
- [42] Komatsu M, Tsuda M, omura S, Oikawa H, Ikeda H, 2008. Identification and functional analysis of genes controlling biosynthesis of 2-methylisoborneol. Proceedings of the National Academy of Sciences 105, 7422–7427. https://doi.org/10.1073/pnas.0802312105
- [43] Andreas MP, Giessen TW, 2024. The biosynthesis of the odorant 2-methylisoborneol is compartmentalized inside a protein shell. Nature Communications 15. https://doi.org/10.1038/s41467-024-54175-4
- [44] Jia Z, Su M, Liu T, Guo Q, Wang Q, Burch M, Yu J, Yang M, 2019. Light as a possible regulator of MIB-producing *Planktothrix* in source water reservoir, mechanism and *in-situ* verification. Harmful Algae 88, 101658. https://doi.org/10.1016/j.hal.2019.101658
- [45] Wang Z, Li R, 2015. Effects of light and temperature on the odor production of 2-methylisoborneol-producing *Pseudanabaena* sp. and geosmin-producing *Anabaena ucrainica* (cyanobacteria). Biochemical Systematics and Ecology 58, 219–226. https://doi.org/10.1016/j.bse.2014.12.013
- [46] Zimba PV, Dionigi CP, Millie DF, 1999. Evaluating the relationship between photopigment synthesis and 2-methylisoborneol accumulation in cyanobacteria. Journal of Phycology 35, 1422–1429. https://doi.org/10.1046/j.1529-8817.1999.3561422.x
- [47] Eisenhoffer GT, Rosenblatt J, 2013. Bringing balance by force: Live cell extrusion controls epithelial cell numbers. Trends in Cell Biology 23, 185–192. https://doi.org/10.1016/j.tcb. 2012.11.006
- [48] Bermudez AG, Latham Z, Hu J, Lin N, 2024. Cell crowding-induced geometric constraint regulates chromatin organizations. Biophysical Journal 123, 407a. https://doi.org/10.1016/j.bpj.2023.11.2493
- [49] Yang S, Golkaram M, Oh S, Oh Y, Cho Y, Yoe J, Ju S, Lalli MA, Park S-Y, Lee Y, Jang J, 2024. ETV4 is a mechanical transducer linking cell crowding dynamics to lineage specification. Nature Cell Biology 26, 903–916. https://doi.org/10.1038/s41556-024-01415-w
- [50] Lawson-Keister E, Manning ML, 2021. Jamming and arrest of cell motion in biological tissues. Current Opinion in Cell Biology 72, 146–155. https://doi.org/10.1016/j.ceb.2021. 07.011

- [51] Drewinko B, Yang LY, Barlogie B, Trujillo JM, 1984. Cultured human tumour cells may be arrested in all stages of the cycle during stationary phase: Demonstration of quiescent cells in G1, s and G2 phase. Cell Proliferation 17, 453–463. https://doi.org/10.1111/j.1365-2184.1984.tb00604.x
- [52] Eisenhoffer GT, Loftus PD, Yoshigi M, Otsuna H, Chien C-B, Morcos PA, Rosenblatt J, 2012. Crowding induces live cell extrusion to maintain homeostatic cell numbers in epithelia. Nature 484, 546–549. https://doi.org/10.1038/nature10999
- [53] Bar J, Cohen-Noyman E, Geiger B, Oren M, 2004. Attenuation of the p53 response to DNA damage by high cell density. Oncogene 23, 2128–2137. https://doi.org/10.1038/sj.onc. 1207325
- [54] Nishio M, Maehama T, Goto H, Nakatani K, Kato W, Omori H, Miyachi Y, Togashi H, Shimono Y, Suzuki A, 2017. Hippo vs. Crab: Tissue-specific functions of the mammalian hippo pathway. Genes to Cells 22, 6–31. https://doi.org/10.1111/gtc.12461
- [55] Sheridan JW, Simmons RJ, 1981. Studies on a human melanoma cell line: Effect of cell crowding and nutrient depletion on the biophysical and kinetic characteristics of the cells. Journal of Cellular Physiology 107, 85–100. https://doi.org/10.1002/jcp. 1041070111
- [56] Tjørve KMC, Tjørve E, 2017. The use of gompertz models in growth analyses, and new gompertz-model approach: An addition to the unified-richards family. PLOS ONE 12, e0178691. https://doi.org/10.1371/journal.pone.0178691
- [57] Lv J, Wang K, Jiao J, 2015. Stability of stochastic richards growth model. Applied Mathematical Modelling 39, 4821–4827. https://doi.org/10.1016/j.apm.2015.04.016
- [58] Peleg M, Cole MB, 1998. Reinterpretation of microbial survival curves. Critical Reviews in Food Science and Nutrition 38, 353–380. https://doi.org/10.1080/10408699891274246
- [59] Wang Y, Zhou JX, Pedrini E, Rubin I, Khalil M, Taramelli R, Qian H, Huang S, 2023. Cell population growth kinetics in the presence of stochastic heterogeneity of cell phenotype. Journal of Theoretical Biology 575, 111645. https://doi.org/10.1016/j.jtbi.2023.111645
- [60] Karim MAU, Aithal V, Bhowmick AR, 2023. Random variation in model parameters: A comprehensive review of stochastic logistic growth equation. Ecological Modelling 484, 110475. https://doi.org/10.1016/j.ecolmodel.2023.110475
- [61] Li Z, Yu J, Yang M, Zhang J, Burch MD, Han W, 2010. Cyanobacterial population and harmful metabolites dynamics during a bloom in yanghe reservoir, north China. Harmful Algae 9, 481–488. https://doi.org/10.1016/j.hal.2010.03.003

- [62] Liang C, Wang D, Yang M, Sun W, Zhang S, 2005. Removal of eathy-must odorants in drinking water by powdered activated carbon. Journal of Environmental Science and Health 40, 767–778. https://doi.org/10.1081/ese-200048262
- [63] Sherr EB, Sherr BF, 1993. Preservation and storage of samples for enumeration of heterotrophic protists. Handbook of Methods in Aquatic Microbial Ecology Lewis Publishers, Boca Raton 207–212
- [64] Komárek J, Anagnostidis K, 1998. Cyanoprokaryota 1. Deu
- [65] Komarek J, Kastovsky J, Mares J, Johansen JR, 2014. Taxonomic classification of cyanoprokaryotes (cyanobacterial genera) 2014, using a polyphasic approach. Preslia 86, 295–335
- [66] Utermöhl H, 1958. Zur vervollkommnung der quantitativen phytoplankton-methodik. Mitteilungen Internationale Vereinigung Für Theoretische Und Angewandte Limnologie 9, 1–38
- [67] R Core Team, 2021. R: A language and environment for statistical computing. R Foundation for Statistical Computing, Vienna, Austria
- [68] Timbers T, Campbell T, Lee M, 2022. R and the tidyverse. In: Data science. Chapman; Hall/CRC, pp 1–26
- [69] Wood SN, 2017. Generalized Additive Models: An introduction with R, 2nd ed. Chapman; Hall/CRC
- [70] Koenker R, Chernozhukov V, He X, Peng L, 2017. Handbook of quantile regression, 1st ed. Chapman; Hall/CRC
- [71] Wickham H, 2009. Introduction. In: ggplot2. Springer New York, pp 1–7
- [72] Liu T, Yu J, Su M, Jia Z, Wang C, Zhang Y, Dou C, Burch M, Yang M, 2019. Production and fate of fishy odorants produced by two freshwater chrysophyte species under different temperature and light conditions. Water Research 157, 529–534. https://doi.org/10.1016/j.watres.2019.04.004
- [73] Perkins RG, Slavin EI, Andrade TMC, Blenkinsopp C, Pearson P, Froggatt T, Godwin G, Parslow J, Hurley S, Luckwell R, Wain DJ, 2019. Managing taste and odour metabolite production in drinking water reservoirs: The importance of ammonium as a key nutrient trigger. Journal of Environmental Management 244, 276–284. https://doi.org/10.1016/j.jenvman.2019.04.123

- [74] Bafford RA, Seagull RW, Chung S, Millie DF, 1993. INTRACELLULAR LOCALIZATION OF THE TASTE/ODOR METABOLITE 2-METHYLISOBORNEOL IN OSCILLATORIA LIMOSA (CYANOPHYTA)1. Journal of Phycology 29, 91–95. https://doi.org/10.1111/j.1529-8817. 1993.tb00285.x
- [75] Pavel M, Renna M, Park SJ, Menzies FM, Ricketts T, Füllgrabe J, Ashkenazi A, Frake RA, Lombarte AC, Bento CF, Franze K, Rubinsztein DC, 2018. Contact inhibition controls cell survival and proliferation via YAP/TAZ-autophagy axis. Nature Communications 9. https://doi.org/10.1038/s41467-018-05388-x
- [76] Li H, Gu X, Chen H, Mao Z, Shen R, Zeng Q, Ge Y, 2022. Co-occurrence of multiple cyanotoxins and taste-and-odor compounds in the large eutrophic lake taihu, china: Dynamics, driving factors, and challenges for risk assessment. Environmental Pollution 294, 118594. https://doi.org/10.1016/j.envpol.2021.118594
- [77] Shi X, Huang Q, Shen X, Wu J, Nan J, Li J, Lu H, Yang C, 2023. Distribution, driving forces, and risk assessment of 2-MIB and its producer in a drinking water source-oriented shallow lake. Environmental Science and Pollution Research 30, 71194–71208. https://doi.org/10.1007/s11356-023-27506-z
- [78] Nan J, Yang C, Yu H, Shi X, Huang Q, Huang J, Li J, 2021. Enclosure culture ban and its effects on water quality and phytoplankton community in a subtropical shallow lake. Aquaculture Research 53, 221–231. https://doi.org/10.1111/are.15568
- [79] Wang M, Yoshimura C, Allam A, Kimura F, Honma T, 2019. Causality analysis and prediction of 2-methylisoborneol production in a reservoir using empirical dynamic modeling. Water Research 163, 114864. https://doi.org/10.1016/j.watres.2019.114864
- [80] Yu C, Shi C, Ji M, Xu X, Zhang Z, Ma J, Wang G, 2019. Taste and odor compounds associated with aquatic plants in taihu lake: Distribution and producing potential. Environmental Science and Pollution Research 26, 34510–34520. https://doi.org/10.1007/s11356-019-06188-6
- [81] Su M, Zhu Y, Andersen T, Wang X, Yu Z, Lu J, Song Y, Cao T, Yu J, Zhang Y, Yang M, 2022. Light-dominated selection shaping filamentous cyanobacterial assemblages drives odor problem in a drinking water reservoir. npj Clean Water 5, 37. https://doi.org/10.1038/s41545-022-00181-2
- [82] Su M, Andersen T, Burch M, Jia Z, An W, Yu J, Yang M, 2019. Succession and interaction of surface and subsurface cyanobacterial blooms in oligotrophic/mesotrophic reservoirs: A case study in Miyun Reservoir. Science of the Total Environment 649, 1553–1562. https://doi.org/J.scitotenv.2018.08.307

- [83] Qi C, Fang J, Wang G, Huang H, Wang Z, Si Z, Zhang L, 2020. Characterization of odorants in contrasting ecotypes of lake taihu: Algae-dominated versus macrophyte-dominated zones. Environmental Science and Pollution Research 27, 42221–42229. https://doi.org/10.1007/s11356-020-07896-0
- [84] Rong C, Liu D, Li Y, Yang K, Han X, Yu J, Pan B, Zhang J, Yang M, 2018. Source water odor in one reservoir in hot and humid areas of southern China: Occurrence, diagnosis and possible mitigation measures. Environmental Sciences Europe 30. https://doi.org/10.1186/s12302-018-0175-8
- [85] Deng X, Qi M, Ren R, Liu J, Sun X, Xie P, Chen J, 2019. The relationships between odors and environmental factors at bloom and non-bloom area in lake taihu, china. Chemosphere 218, 569–576. https://doi.org/10.1016/j.chemosphere.2018.11.121